mathematics

MDPI

Article

Design of a Novel Chaotic Horse Herd Optimizer and Application to MPPT for Optimal Performance of Stand-Alone Solar PV Water Pumping Systems

Rabeh Abbassi [1,2,3,*] and Salem Saidi [2,4]

[1] Department of Electrical Engineering, College of Engineering, University of Ha'il, Ha'il City 81451, Saudi Arabia
[2] LaTICE Laboratory, Higher National Engineering School of Tunis (ENSIT), University of Tunis, 5 Avenue Taha Hussein, P.O. Box 56, Tunis 1008, Tunisia
[3] Institute of Applied Sciences and Technology of Kasserine (ISSATKas), University of Kairouan, P.O. Box 471, Kasserine 1200, Tunisia
[4] National School of Advanced Sciences and Technologies of Borj Cedria (ENSTAB), University of Carthage, P.O. Box 122, Hammam-Chott 1164, Tunisia
* Correspondence: r.abbassi@uoh.edu.sa

Abstract: A significant part of agricultural farms in the Kingdom of Saudi Arabia (KSA) are in off-grid sites where there is a lack of sufficient water supply despite its availability from groundwater resources in several regions of the country. Since abundant agricultural production is mainly dependent on water, farmers are forced to pump water using diesel generators. This investigation deals with the increase in the effectiveness of a solar photovoltaic water pumping system (SPVWPS). It investigated, from a distinct perspective, the nonlinear behavior of photovoltaic modules that affects the induction motor-pump because of the repeated transitions between the current and the voltage. A new chaotic Horse Herd Optimization (CHHO)-based Maximum Power Point Tracking technique (MPPT) is proposed. This algorithm integrates the capabilities of chaotic search methods to solve the model with a boost converter to maximize power harvest while managing the nonlinear and unpredictable dynamical loads. The analytical modeling for the proposed SPVWPS components and the implemented control strategies of the optimal duty cycle of the DC–DC chopper duty cycle and the Direct Torque Control (DTC) of the Induction Motor (IM) has been conducted. Otherwise, the discussions and evaluations of the proposed model performance in guaranteeing the maximum water flow rate and the operation at MPP of the SPVWPS under partial shading conditions (PSC) and changing weather conditions have been carried out. A comparative study with competitive algorithms was conducted, and the proposed control system's accuracy and its significant appropriateness to improve the tracking ability for SPVWPS application have been proven in steady and dynamic operating climates and PSC conditions.

Keywords: metaheuristic optimization; artificial intelligence; solar photovoltaic water pumping; Saudi Vision 2030; smart irrigation systems; power reliability and energy efficiency; maximum power point tracking; sustainable agriculture

MSC: 68T20; 39A33

Citation: Abbassi, R.; Saidi, S. Design of a Novel Chaotic Horse Herd Optimizer and Application to MPPT for Optimal Performance of Stand-Alone Solar PV Water Pumping Systems. *Mathematics* **2024**, *12*, 594. https://doi.org/10.3390/math12040594

Academic Editor: Kotb Basem Tawfiq

Received: 16 January 2024
Revised: 15 February 2024
Accepted: 15 February 2024
Published: 17 February 2024

1. Introduction

1.1. Motivation

During recent decades, the growth of global electricity consumption has been and is still very remarkable. It is an expected consequence of the rapid development of industry and other sectors that are strongly linked to energy generation. Today, a significant part (71%) of electricity is produced from non-renewable energy resources (*RERs*) such as coal, natural gas, oil, uranium, and water [1]. The major problem with such conventional exhaustible resources is that their regeneration rate is extremely slow on a human lifetime scale, as they require millions of years to be formed. Faced with these dilemmas, the growth in energy demand, and the risk of overuse of these resources, a significant increase in the world price of oil is increasingly experienced. However, this type of energy consumption has negative impacts on the environment. In fact, the important emission of greenhouse gases plays a decisive role in climate change and the increase in pollution and temperature around the world. As a result, the world's attention has been focused on alternative solutions to limit any adverse environmental impacts. For example, the development of non-polluting energy resources based on renewable energies, which have the advantage of natural and indefinite regeneration on the time scale of our civilization, is being increasingly emphasized. For its own part, the energy from the Sun alone currently meets these criteria of both abundance on the surface of the Earth and infinite regeneration. Solar energy can be used directly in thermal form or after conversion into electrical energy via photovoltaic (PV) cells.

In the agricultural sector, which includes various activities that, in some sense, constitute the main economic engine of several countries, most solar energy applications are direct, such as photosynthesis, drying, heating applications, etc., or indirect, such as irrigation, water desalination, and various other applications. In particular, the groundwater resources available in Saudi Arabia (especially in Hail), which are not yet well exploited for irrigation, need to be rationalized. Moreover, these water resources are usually extracted artificially for the irrigation of cultivated vegetation to increase their productivity and allow their normal development in the event of a water deficit induced by rainfall. Pumping groundwater requires the use of electricity, which is not widely available in all desert and remote sites. One solution is, therefore, to use an available renewable source, such as solar photovoltaic energy, to pump water since non-renewable resources are exhaustible and polluting. The geographical location of Hail promotes the development of solar PV energy use. Indeed, due to the high intensity of radiation received, the region of Hail, the pioneer of the use of solar energy in the Kingdom, can cover some of its needs with solar energy. These advantages could be beneficial in the most remote areas, especially in the application of water pumping in the agricultural sector. Consequently, with the KSA's trends to decrease water consumption and further develop the agricultural sector and green energy, the development of sustainable agriculture is an objective investment in accordance with Vision 2030. In this context, the objective of this study is to investigate the innovation of a pilot program that aims to highlight opportunities for sustainable agriculture in the Hail region using a smart water pumping system controlled by artificial intelligence (AI) and powered by a solar photovoltaic generator. The contribution of this project is the proposal of a feasibility study and smart control based on AI techniques and new bioinspired metaheuristic optimization algorithms. This skill will be helpful in guaranteeing a sufficiently autonomous and flexible smart system that can ensure service continuity and contribute to the advancement of sustainable agriculture while saving water, energy, and the environment and ensuring reliability and efficiency.

1.2. Literature Review and Related Works

The availability and use of energy are increasingly critical for the social and economic development of societies and are the primary resources for improving human life. In 2020, approximately one billion people worldwide live in small and remote villages that do not have access to electricity from power grids [2]. In many cases, extending the distribution grid is unachievable because of the dispersed population or rugged terrain; therefore, standalone power systems are emerging as the most viable options. In particular, the agricultural sector, on which food security and nutrition depend, is a major consumer of natural resources such as land, soil, water, and energy. This sector depends on energy to ensure the growing, transporting, and processing of crops and livestock. Conventional non-renewable fuels (coal, oil, and natural gas) are the most widely used in the current agricultural sector [3]. However, this primary energy source, whose resources have become very depleted, emits large amounts of greenhouse gases that are responsible for climate change. To address this critical challenge, Saudi Arabia, like many other developed countries around the world, has chosen renewable energy as a good alternative according to the Vision 2030 guidelines [4]. The combination of several renewable energy resources, such as hybrid wind-PV systems and conventional diesel generators with or without the use of battery storage, is a cost-effective and environmentally friendly source of electricity generation that is being commercialized over the long term. In particular, solar energy in Saudi Arabia is considered the most capable renewable source of energy for rapid, sustainable agricultural development, mainly in rural desert areas [5]. Modern, well-designed, simple to maintain, and cost-effective solar PV systems can provide the necessary energy whenever needed. The Sun is an economical and useful source of energy with a good level of safety and environmental friendliness [6]. One of the applications of photovoltaic system technology without polluting emissions and without the need for fuel is the provision of the energy needed for irrigation and the promotion of sustainable agriculture in rural areas [7].

Increasing attention is currently being devoted to studies that have led to progress in the application of photovoltaic systems to cover a load of agricultural operations such as animal farming, heating and cooling of the dairy farm, pumping water for drinking water supply and agricultural irrigation... [8,9]. Many researchers have studied the use of these systems. Everest [10] presented a comprehensive study on the forms of renewable energy and the potential for its exploitation by the Turkish agricultural industry. Mahto [11] conducted a similar study in India to develop the use of renewable energy to promote sustainable agriculture. To simultaneously generate renewable electricity and reduce water evaporation at the same time, Ravichandran et al. [12] investigated an innovative floating photovoltaic cover for irrigation reservoirs. Mazhar et al. [13] investigated the techno-economic factors influencing the adoption of renewable energy in the Gilgit–Baltistan region of Pakistan. Irfan et al. also examined the feasibility of using solar heating systems to reduce energy consumption of poultry farms [14]. Many other studies have investigated the use of renewable energy in farms, such as in the design of a PV-pumped water irrigation system for crops in the Algerian Sahara region. Other studies have been developed in the same context of solar energy in farms, reliability, feasibility, and economic assessments in various case studies for PV systems, either grid-connected or stand-alone [15,16]. To further advance research in this field in terms of modeling, simulation, sizing, economic analysis, and in particular optimization, various software tools such as HOMER, Hybrid2, RETScreen, iHOGA, Hyb Swim, and HySys have been developed [17]. More recently, Filipe Pereira et al. [18] elaborated a complete study of a smart farm including several phases (economic study, control, monitoring, and introduction of the PV system). The results showed that a reduction of 83.2% of the grid energy can be achieved using the photovoltaic system, with a CO_2 savings of 5527 kg and an investment yield of approximately 8 years. In addition, Sangeetha B. P. et al. [19] introduced an intelligent farm management system to improve agricultural benefits and crop production. Thus, the method fulfills all its objectives in terms of water consumption, total operating costs, labor reduction, energy consumption, and productivity. Other studies [20] have provided methodologies for sizing smart PV irrigation systems. The numerical results show that the presented methods led to improved irrigation scheduling and, consequently, improved utilization compared to conventional approaches.

In solar PVWPSs, optimizing PV power extraction is a crucial task. The performance of a PV Generator (PVG) is considerably influenced by meteorological conditions and the phenomena that affect them, such as partial shading and dust accumulation. As a result, the global peak of the voltage/power (P-V) characteristic can fluctuate, and even multiple local peaks can be detected [21,22]. These and other phenomena lead to a significant reduction in the power produced by the PVG and affect its lifespan. To address this issue and counteract such impacts with the aim of optimally harvesting the maximum available power from the PV system, a series of studies have been proposed [23,24]. In particular, metaheuristic-based approaches have been widely used such as Particle Swarm Optimization (PSO) [25], Extended Grey Wolf Optimizer (EGWO) [26], Moth flame optimization (MFO) [27], Spider Monkey Optimization (SMO) [28] , Honey Badger Optimizer (HBO) [29], Hunter Pray Optimizer (HPO) [30], and Arithmetic Optimization Algorithm (AOA) [31].

These research initiatives are aimed at improving the efficiency of PV systems by adopting the principle of Maximum Power Point Tracking (MPPT). As their name implies, MPPT techniques allow one to extract the maximum power that the PVG can deliver. Over the years, the investigation of robust MPPT methods for tracking the Maximum Power Point (MPP) of PV systems has been the focus of several research studies. These research initiatives are aimed at improving the efficiency of PV systems by adopting the principle of Maximum Power Point Tracking (MPPT). As their name implies, MPPT techniques allow one to extract the maximum power that the PVG can deliver. Over the years, the investigation of robust MPPT methods for tracking the Maximum Power Point (MPP) of PV systems and wind energy conversion systems has been the focus of several research studies [32].

Although these approaches are designed for the same purpose, they differ significantly in terms of performance, tracking speed, software complexity, hardware implementation, steady-state oscillations, and whether the overall MPP is accurately tracked during rapid changes in meteorological conditions. To bring this topic closer to PVWPS applications, researchers have investigated this subject worldwide. In [33], three MPPT controls based on Variable Step Size Perturb and Observe (VSS-P&O), Variable Step Size Incremental conductance (VSS-INC), and a Kalman filter (KF) were used in combination with DTC to optimize the control of a PVWPS equipped with a multilevel inverter and IM. It has been shown that in the case of abrupt changes in irradiance, KF-MPPT performed better than VSS-P&O and VSS-INC in terms of temporal response and power oscillation. Another study [34] investigated the economic and environmental benefits of a PVWPS through optimal MPPT based on genetic algorithms to assess its ability to meet the energy needs for irrigation in the Meknes region of Morocco. Two coupling methods for the solar generator were analyzed and discussed. Ahmed et al. [35] conducted some performance evaluations of the prediction of the duty cycle of a DC–DC converter to allow the optimization of the water flow rate of a PVWPS by ensuring its operation at MPP under changing atmospheric conditions. In the context of meeting the water needs of rural areas, a PVWPS encompassing a high-gain boost DC–DC chopper controlled by a Semi Pilot Cell-based Fractional Open Circuit Voltage (SPC-FOCV) MPPT and an inverter driving a Permanent Magnet Synchronous Motor (PMSM)-Pump Assembly by Space Vector Modulation (SVM) technique was proposed in [36,37]. In [38], a sensorless speed control approach was proposed to improve the efficiency and reliability of PVWPS in real-world applications. The proposed system combines a PV Generator (PVG) and a three-phase induction motor, both driven by adaptive power control to determine the maximum power point of the PVG and the input reference speed for the DTC control. The overall control process operates as a closed-loop system without a speed sensor because the speed estimation is provided by the Extended Kalman–Bucy filter. The integration of AI theories has been exploited to increase the efficiency of a PVWPS using a radial basis function neural network (RBFNN) driving a single-ended primary inductor converter (SEPIC) to ensure MPPT of the PV generator, and then feeding a brushless DC (BLDC) motor through a voltage source inverter (VSI) [39]. Various performance indicators, such as the MPP settling time, current ripple, voltage ripple, average power loss, torque ripple, and total harmonic distortion (THD) of the stator current, have been investigated to prove the efficiency of the control system. The authors of [40] developed an application of a PVWPS equipped with a three-phase induction motor without a DC–DC converter. The daily amount of pumped water has been increased to a higher level, reaching approximately 80%, regardless of environmental variations.

In the same respect as the reviewed works, this research falls within the framework of an innovative project aimed at highlighting the potential of photovoltaic pumping driven by artificial intelligence techniques to cover water needs and its contribution to the development of sustainable local agriculture in the Hail region.

1.3. Contributions and Outline

The Horse Herd Optimization (HHO) algorithm is a novel nature-inspired algorithm developed by MiarNaeimi et al. [41]. It imitates the horses' herding behavior. Such behavior mimics the social life of horses by exploring six key features: the grazing process, herd hierarchy, sociability between members, imitation of observed behaviors, defense mechanisms, and roam nature. The carefully selected HHO has been persuaded by its various features, in contrast to competitive metaheuristic optimizers, even for the MPPT problem [42]. The favorable performance of this algorithm can be explained as follows.

- Regular classification of search agents according to their location and fitness.
- Powerful leadership process by decreasing the number of search particles and the continuous improvement of the state of the particles during each classification.
- Simultaneous exploitation of the six key behaviors to adjust the horse herd's performance.
- Low computational cost through speed sorting exploitation in MATLAB.
- Harmonious relationships between the horses' motion guaranteeing the HHO high performance.
- Accurate convergence to the best solution through efficient trade-off between exploration and exploitation.

Considering the significant properties of the chaos theory that enable the maintenance of population diversity and, consequently, the ability to improve the quality of the global optimum search and escape falling into a local optimum when dealing with complicated problems, a new chaotic HHO (CHHO) optimizer has been proposed to address the aforementioned issue.

Within this framework, the main contributions of the present study are revealed below.

- To propose and implement the CHHO optimizer to tackle the challenge of the DC–DC chopper control via the tracking of the maximum power to optimize a solar PV water pumping system.
- To carry out an enriching comparative analysis study of the CHHO performance and those of Perturb and Observe (P&O), Particle Swarm optimizer (PSO), and original HHO when implemented, taking into account the same assumptions.
- To assess the performance of the proposed CHHO in steady and dynamic operating climates, as well as under PSC conditions compared to these algorithms.
- To highlight the distinction of the proposed CHHO in terms of accuracy, stability, speed, power efficiency, and water flow rate.

The mathematical representation of the system studied is presented in Section 2. It explains the modeling and design of the PVWPS components and control systems, as well as the proposed CHHO-MPPT method. Section 3 describes the simulation and analysis of the results, and the work is concluded in Section 4.

2. Modeling and Design of the Solar Photovoltaic-Powered Pumping System

To harvest the groundwater, the pumping system ensures that the water is transported and circulated to different use points. In the present work, the investigated system is a renewable energy source-based water pumping system without energy storage. It consists of a centrifugal water pump driven by a three-phase induction motor powered by a photovoltaic generator. The adaptation stage between the load and the PV power source consists of a series combination of a boosted DC–DC chopper and a three-phase, three-arm voltage source inverter. The chopper is controlled by a Maximum Power Point Tracking (MPPT) technique to ensure maximum power extraction to the load. The VSI inverter is controlled by the DTC approach, which synthesizes three controllers: one for speed control and two others for direct and quadratic stator currents control. In this context, the main challenge is to control a complex sixth-order system with a high degree of nonlinearity. Figure 1 shows the synoptic diagram of the photovoltaic pumping system.

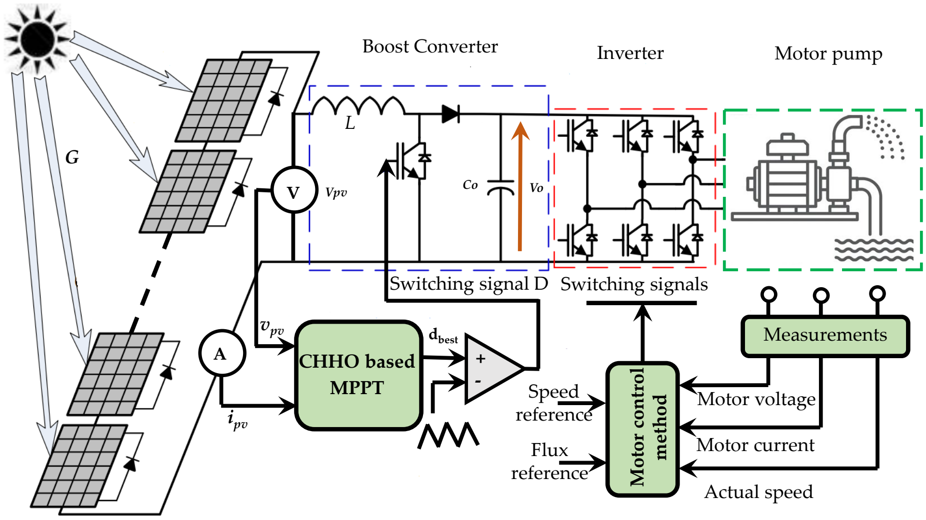

Figure 1. Stand-alone solar photovoltaic water pumping system schematic diagram.

2.1. Solar PV Generator Modeling

When illuminated, a PV cell generates a current I proportional to the irradiance it receives. During its operation, it behaves like a diode. It flows a diode current I_D when connected to a load. Figure 2 shows the equivalent electrical diagram of a photovoltaic cell.

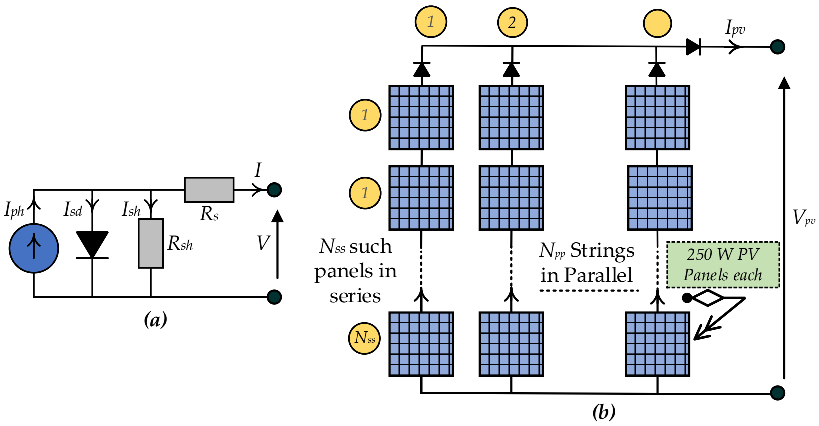

Figure 2. PV system: (**a**) Equivalent circuit of single-diode model. (**b**) PV array configuration.

According to the model illustrated in Figure 2, the relationships between the flowing currents can be expressed as shown in expression (1):

$$I = I_{ph} - I_{sd}\left[e^{\left(\frac{V+IR_s}{\eta V_t}\right)} - 1\right] - \frac{V + IR_s}{R_{sh}} \tag{1}$$

Herein, I_{ph} is the photocurrent generated, I_{sd} is the diode reverse saturation current, N_s is the number of cells connected in series, R_{sh} is the shunt resistor, R_s is the series resistor and V_t is the temperature voltage given by Equation (2), where η is the diode ideality factor, k is Boltzmann's constant, T is the temperature of the P-N junction, and q is the charge of an electron.

$$V_t = \frac{\eta kT}{q} \tag{2}$$

To meet the power requirements, the PV generator consists of a set of N_{ss} panels in series with a set of N_{pp} panels in parallel. Therefore, the characteristic equation of a PV generator is given in Equation (3)

$$I_a = N_p I_{ph} - N_p I_{sd} \left[e^{\left(\frac{V + I R_s N_s \left(\frac{N_{ss}}{N_{pp}} \right)}{N_{ss} V_t} \right)} - 1 \right] - \frac{V + I R_s N_s \left(\frac{N_{ss}}{N_{pp}} \right)}{\left(\frac{N_{ss}}{N_{pp}} \right) R_{sh}} \tag{3}$$

The parameters of the chosen module are summarized in Table 1.

Table 1. The key specifications of the Solar SunPower SPR-X20-250-BLK PV module.

Parameter	Value
Open circuit voltage (V_{oc})	50.93 V
Voltage at maximum power point (Vmp)	42.8 V
Short circuit current (Isc)	6.2 A
Current at maximum power point (Imp)	5.84 A
Maximum power at STC ($Pmax$)	249.952 W
Number of cells connected in series	72
Temperature coefficient of Isc	0.013306 A/°C
Temperature coefficient of Voc	−0.291 V/°C

The current versus voltage (V-I) and power versus voltage (P-V) characteristics depend essentially on the irradiance and temperature of the photovoltaic generator. This dependence is shown in Figure 3. Clearly, a change in irradiance, Figure 3a,b, and temperature, Figure 3c,d, results in a change in the maximum power point, which deviates from its location as meteorological conditions change.

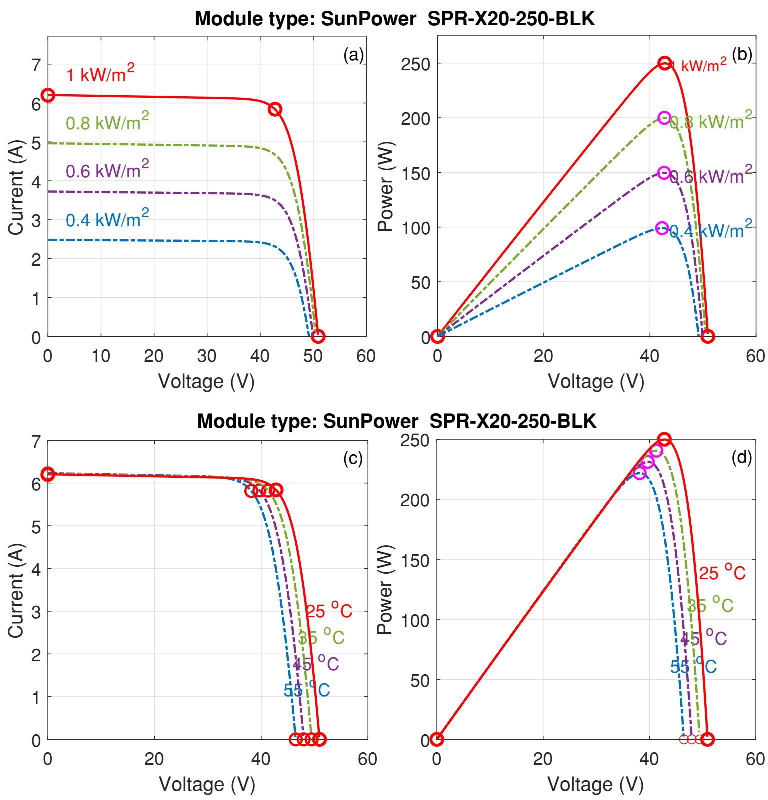

Figure 3. Influence of irradiance and temperature changes on I-V and P-V characteristics: (**a**,**b**) Effect of irradiance; (**c**,**d**) Effect of temperature.

2.2. Modeling of the DC/DC Converter

The PV Generator (PVG) is connected to the DC bus via a boost chopper driven by an MPPT control system (see Figure 2). This converter acts as a matching stage between the GPV output voltage and the DC bus voltage. The chopper's operating cycle can be divided into two distinct time intervals. The first interval, from zero to "αT", is characterized by the turn-on of the controlled switch and the blocking of the diode. Applying KIRCHOFF's laws, the main equations characterizing the converter in the "ON" state are given by the following system (Equation (4)):

$$\begin{cases} V_{pv} = L\frac{dI_{pv}}{dt} \\ I_o = -C_o\frac{dV_o}{dt} \end{cases} \tag{4}$$

During the second cycle interval, from "αT" to "T", the controlled switch is "OFF" and the diode is "ON". The boost chopper is thus described by the following system of Equation (5):

$$\begin{cases} V_{pv} = L\frac{dI_{pv}}{dt} + V \\ I_o = I_{pv} - I_{Co} \end{cases} \tag{5}$$

On the basis of the two previously developed equation systems, the mathematical model of the boost DC–DC converter is derived through the following relationships (Equations (6) and (7)):

$$V_{pv} = D\left(L\frac{dI_{pv}}{dt}\right) + (1-D)\left(L\frac{dI_{pv}}{dt} + V_o\right) \tag{6}$$

$$I_o = D\left(-C_o\frac{dV_o}{dt}\right) + (1-D)(I_{pv} - I_{Co}) \tag{7}$$

with D the duty cycle of the converter. Therefore, based on the previous equations, the voltage and current expressions below are deduced:

$$V_{pv} = L\frac{dI_{pv}}{dt} + (1-D)V_o \tag{8}$$

$$I_o = C_o\frac{dV_o}{dt} + (1-D)I_{pv} \tag{9}$$

In this study, the dynamic duty cycle D is achieved using the MPPT control, which will be the subject of a later section.

The pumping system control is organized into two distinct aspects: (i) the Maximum Power Point Tracking (MPPT) control for the PVG, and (ii) the Direct Torque Control (DTC) of the Induction Motor (IM) speed.

2.3. DTC Control Strategy of the IM

Figure 4a presents the block diagram of a sensorless Direct Torque Control (DTC) drive. The diagram encompasses two flux and torque comparators, a switching strategy responsible for generating the switching signals for the voltage source inverter (VSI), and a torque and stator flux observer [43]. The fundamental concept of the DTC strategy can be summarized as follows: during each sampling period, the selection of the optimal voltage vector aims to rapidly minimize the errors in torque and flux magnitude [37,44]. The right application of this principle allows fast and decoupled control of torque and flux without Pulse Width Modulation (PWM) or current control [45]. As can be seen in Figure 4a, the error between the estimated torque T_e and the reference torque T_e^* is the input of a three-level hysteresis comparator which is shown in Figure 4b. The error between the estimated stator flux magnitude φ_s and the reference stator flux magnitude φ_s^* is the input of a two-level hysteresis comparator, which is shown in Figure 4c.

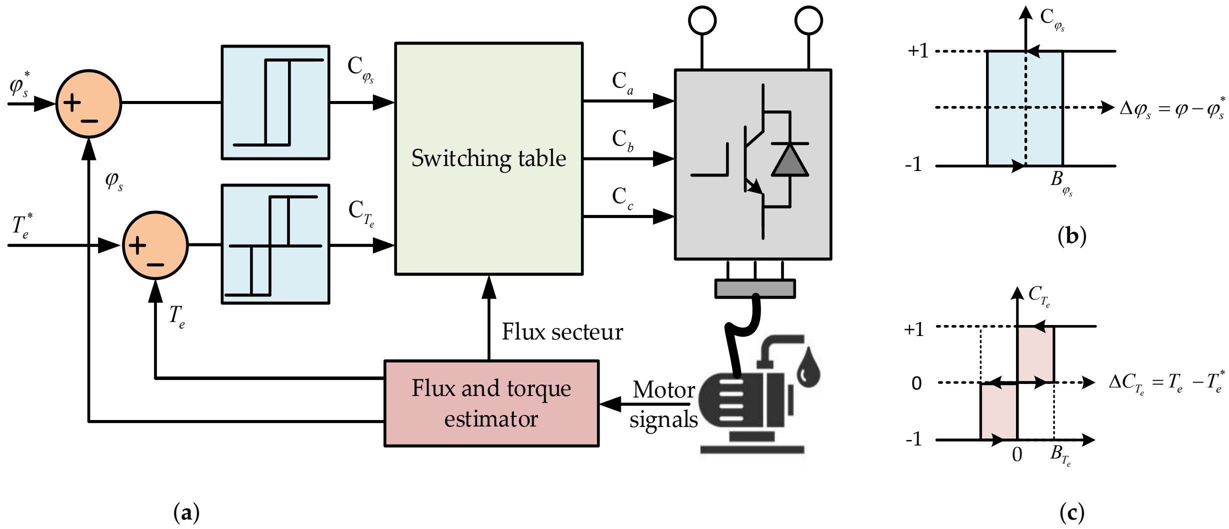

Figure 4. Block diagram of the DTC scheme for IM. (**a**) Overall block diagram of DTC. (**b**) Flux hysteresis comparator. (**c**) Torque hysteresis comparator.

The mathematical representation of an induction motor can be accomplished by utilizing the equations of the stator current vector and rotor flux vector. The induction machine state space model in the (d, q) frame, which is derived from the Equation (10):

$$\begin{bmatrix} \frac{di_{ds}}{dt} \\ \frac{di_{qs}}{dt} \\ \frac{d\varphi_{dr}}{dt} \\ \frac{d\varphi_{qr}}{dt} \end{bmatrix} = \begin{bmatrix} -\left(\frac{1}{\tau_s\sigma} + \frac{1-\sigma}{\tau_r\sigma}\right) & \omega_s & \frac{1-\sigma}{\tau_r L_m\sigma} & \frac{1-\sigma}{L_m\sigma}\omega \\ -\omega_s & -\left(\frac{1}{\tau_s\sigma} + \frac{1-\sigma}{\tau_r\sigma}\right) & \frac{1-\sigma}{L_m\sigma}\omega & \frac{1-\sigma}{\tau_r L_m\sigma} \\ \frac{L_m}{\tau_r} & 0 & -\frac{1}{\tau_r} & (\omega_s - \omega) \\ 0 & \frac{L_m}{\tau_r} & -(\omega_s - \omega) & -\frac{1}{\tau_r} \end{bmatrix} \begin{bmatrix} i_{ds} \\ i_{qs} \\ \varphi_{ds} \\ \varphi_{qs} \end{bmatrix} + \begin{bmatrix} \frac{1}{\sigma L_s} & 0 \\ 0 & \frac{1}{\sigma L_s} \\ 0 & 0 \\ 0 & 0 \end{bmatrix} \begin{bmatrix} V_{ds} \\ V_{qs} \end{bmatrix} \tag{10}$$

where V_{ds} and V_{qs} are the direct and quadrature voltages in the (d, q) reference frame, i_{ds} and i_{qs} are the direct and quadrature stator currents, φ_{dr} is the direct component of the magnetic flux of the rotor, φ_{qr} is its quadrature component, ω_s is the stator pulsation, ω is the pulsation corresponding to the mechanical rotational speed, L_m, L_r, and L_s are the mutual, rotor, and stator self inductances, respectively. τ_r and τ_s are the stator and rotor time constants, respectively. R_s is the stator resistance of the induction machine, and σ is the leakage factor given by (11):

$$\sigma = \left(1 - \frac{L_m}{L_r L_s}\right) \tag{11}$$

In the stationary reference frame, after measuring the stator voltages and currents, the derivatives of the stator flux components are (12) and (13):

$$\frac{d\varphi_{s\alpha}}{dt} = V_{s\alpha} - R_s i_{s\alpha} \tag{12}$$

$$\frac{d\varphi_{s\beta}}{dt} = V_{s\beta} - R_s i_{s\beta} \tag{13}$$

where R_s is the phase stator resistance. The magnitude of the stator flux (φ_s) is expressed as follows (14):

$$\varphi_s = \sqrt{\varphi_{s\alpha}^2 + \varphi_{s\beta}^2} \tag{14}$$

The two voltage components $V_{s\alpha}$ and $V_{s\beta}$, in the (α, β) reference frame, are calculated from the commands (C_a, C_b and C_c) and the voltage measurement (E_d) as follows (15) and (16):

$$V_{s\alpha} = \sqrt{\frac{2}{3}} E_d \left(C_a - \frac{1}{2}(C_b + C_c) \right) \tag{15}$$

$$V_{s\beta} = \sqrt{\frac{1}{2}} E_d (C_b - C_c) \tag{16}$$

In Equations (17) and (18), the two components of (φ_r) in the (α, β)reference frame are computed.

$$\varphi_{r\alpha} = \frac{L_r}{L_m} (\varphi_{s\alpha} - \sigma L_s i_{s\alpha}) \tag{17}$$

$$\varphi_{r\beta} = \frac{L_r}{L_m} \left(\varphi_{s\beta} - \sigma L_s i_{s\beta} \right) \tag{18}$$

Accordingly, the electromagnetic torque is equated as in Equation (19):

$$T_e = p\left(\varphi_{s\alpha} i_{s\alpha} - \varphi_{s\beta} i_{s\beta}\right) \tag{19}$$

The mechanical equation of the induction machine driving a load is expressed by Equation (20):

$$T_e - T_{pump} = J \frac{d}{dt}\omega + f\omega \tag{20}$$

where J is the moment of inertia f is the coefficient of viscous friction. The resistive torque exerted by the centrifugal pump can be described.

As such, the mechanical equation of the AC induction machine and the load (pump) can be rewritten as below (21):

$$T_{pump} = a + b\omega + c\omega^2 + e\omega^3 \tag{21}$$

where ω is the angular velocity and "a", "b", "c", and "e" are the practical characteristic of the pump taken from the ETAP11 software [46]. Table 2 lists the electric data, including the main parameters and characteristics of the IM motor.

Table 2. The key specifications of the three-phase induction motor.

Parameter	Value
Rated Power	1.5 W
Rated Voltage	380 V
Stator resistance (R_s)	4.85 Ω
Rotor resistance (Rr)	3.805 Ω
Stator leakage inductance (Ls)	0.274 H
Rotor leakage inductance(Lr)	0.274 H
Magnetizing inductance (M)	0.258 H
Moment of Inertia J	0.02 kg·m^2
Friction f	0.01 kg^2·s^{-1}
Number of poles p	2

The sector can be selected based on the position of the estimated stator flux, which can be obtained from the $\alpha-$ and β-axis stator flux components, as Equation (22) shows below:

$$\theta = \tan^{-1}\left(\frac{\varphi_\beta}{\varphi_\alpha}\right) \tag{22}$$

where θ presents the angle of stator flux. The regulation of the flux is conducted using a two-level digital output hysteresis-controller according to the relations given below (23):

$$C_{\varphi_s} = \begin{cases} 1 & \Delta\varphi_s = \varphi_s - \varphi_{s^*} \leq B_\varphi \\ 0 & \Delta\varphi_s = \varphi_s - \varphi_{s^*} > B_\varphi \end{cases} \tag{23}$$

The torque is also regulated by a hysteresis-controller. The difference is that it has three levels of digital outputs as follows (24):

$$C_{T_e} = \begin{cases} 1 & \Delta C_{T_e} = T_e - T_{e^*} > B_{T_e} \\ 0 & \Delta C_{T_e} = T_e - T_{e^*} = 0 \\ -1 & \Delta C_{T_e} = T_e - T_{e^*} < -B_{T_e} \end{cases} \tag{24}$$

Table 3 presents the Optimum Switching Vector Selection Table, which illustrates the recommended selection of switching vectors in all sectors of the stator flux plane [43]. This table is constructed based on the values of the stator flux error status, the torque error status, and the orientation of the stator flux for the counterclockwise rotation of the shaft.

Table 3. Switching table for DTC.

Sector		1	2	3	4	5	6
$C_{\varphi_s=-1}$	$C_{Te} = -1$	$\bar{V}_2$	$\bar{V}_3$	$\bar{V}_4$	$\bar{V}_5$	$\bar{V}_6$	$\bar{V}_1$
	$C_{Te} = 0$	$\bar{V}_7$	$\bar{V}_0$	$\bar{V}_7$	$\bar{V}_0$	$\bar{V}_7$	$\bar{V}_0$
	$C_{Te} = +1$	$\bar{V}_6$	$\bar{V}_1$	$\bar{V}_2$	$\bar{V}_3$	$\bar{V}_4$	$\bar{V}_5$
$C_{\varphi_s=+1}$	$C_{Te} = -1$	$\bar{V}_3$	$\bar{V}_4$	$\bar{V}_5$	$\bar{V}_6$	$\bar{V}_1$	$\bar{V}_2$
	$C_{Te} = 0$	$\bar{V}_0$	$\bar{V}_7$	$\bar{V}_0$	$\bar{V}_7$	$\bar{V}_0$	$\bar{V}_7$
	$C_{Te} = +1$	$\bar{V}_5$	$\bar{V}_6$	$\bar{V}_1$	$\bar{V}_2$	$\bar{V}_3$	$\bar{V}_4$

2.4. CHHO-Based MPPT Control of the Boost DC–DC Converter

2.4.1. Horse Herd Optimization Algorithm (HHO)

The Horse Herd Optimization Algorithm (HHO) is a very advanced swarm-based optimization technique [41]. This algorithm is inspired by the investigation and analysis of social behavior patterns of horses in their natural environment. It is recognized that, depending on the age of the horses, their social behavior is mainly limited to the following six main patterns:

- Grazing (G): Horses are considered grazing animals par excellence, as they spend most of their time on the pasture eating grasses and forages.
- Hierarchy (H): In the wild, the hierarchy of a herd of horses and the commitment of each horse to its rank help to reduce aggressive behavior.
- Social communication (S): Horses communicate within their herds in a variety of ways, making it easier for them to persist in groups.
- Imitation (I): Whatever the typical behavior of horses living in a group, group communication between them leads to imitation of each other's behavior.
- Defense mechanism (D): Because of their tremendous speed, horses generally react to threats by running away; in other cases, they stay in their territory and defend other members of the herd.
- Roaming (R): In the wild, horses like to spend their time roaming, grazing grass, and changing locations to discover new places.

Thus, independently of their ages, the movement of the horses at each iteration is simulated according to the six aforementioned behaviors in accordance with Equation (25):

$$\vec{X}_m^{(iter,AGE)} = \vec{V}_m^{(iter,AGE)} + \vec{X}_m^{(iter,AGE)}, \quad AGE = \alpha, \beta, \gamma, \delta \tag{25}$$

where $\vec{X}_m^{(iter,AGE)}$ specifies the position of the m^{th} horse, AGE represents the age range of the horse under consideration, $iter$ is the iteration number and $\vec{V}_m^{(iter,AGE)}$ shows the velocity vector associated with this horse.

In general, the average lifespan of a horse is estimated at 25–30 years, and it may live more or less than that period depending on multiple factors related, especially to genetics, food, and lifestyle. One of the most important basics of this algorithm is dividing the horses in the flock. In fact, the classification is made by determining the ages of horses according to frequency based on the following: The first group, called δ, includes horses that are between 0 and 5 years old. The second group, called γ, includes horses that are between 5 and 10 years old. The third group, called β, includes horses that are between 10 and 15 years old. The fourth group, called α, includes horses that are older than 15 years.

The selection of the horses' age responses matrix should be sorted during each iteration. For any iteration, the horse ages are chosen according to these rules: the α group of horses represents the top 10% of the ranged population, and the next 20% of the members (horses) are designated as β. γ members are the subsequent 30%, and the age of the remaining 40% is retained as δ.

To materialize the speed vector mathematically, taking into account the behaviors of the different categories of horses, the motion vector of the horses at each HHO step is represented by the following Equation (26):

$$\begin{aligned}
\vec{V}_m^{(iter,\alpha)} &= \vec{G}_m^{(iter,\alpha)} + \vec{D}_m^{(iter,\alpha)} \\
\vec{V}_m^{(iter,\beta)} &= \vec{G}_m^{(iter,\beta)} + \vec{H}_m^{(iter,\beta)} + \vec{S}_m^{(iter,\beta)} + \vec{D}_m^{(iter,\beta)} \\
\vec{V}_m^{(iter,\gamma)} &= \vec{G}_m^{(iter,\gamma)} + \vec{H}_m^{(iter,\gamma)} + \vec{S}_m^{(iter,\gamma)} + \vec{I}_m^{(iter,\gamma)} + \vec{D}_m^{(iter,\gamma} + \vec{R}_m^{(iter,\gamma)} \\
\vec{V}_m^{(iter,\delta)} &= \vec{G}_m^{(iter,\delta)} + \vec{I}_m^{(iter,\delta)} + \vec{R}_m^{(iter,\delta)}
\end{aligned} \tag{26}$$

- Grazing step (GS):

Recognizing the horse as an herbivore may seem obvious. However, grazing is essential for horses from a nutritional, locomotor, and behavioral point of view. When grazing, the amount of nutrients the horse can extract from the grass depends on its ability to eat it. In fact, the ingestion capacity is a function of two factors: the time the horse spends grazing over a 24-h period (between 16 and 20 h) and the speed at which it grazes. Otherwise, the quality and digestibility of grass is constantly evolving: it is often too high in relation to the horse's needs in spring and can become insufficient in very dry summer. In this case, the horses' high-performance incisors enable them to cut the vegetation at ground level to compensate in part for this scarcity and to increase the speed of ingestion and the grazing area.

Considering the importance of grazing for horses from different ages, the mathematical expression of the grazing is expressed mathematically as per the Equations (27) and (28).

$$\vec{G}_m^{(iter,AGE)} = g_{iter}(\tilde{u} + p\tilde{l})[X_m^{(iter-1)})], \quad AGE = \alpha, \beta, \gamma and \delta \tag{27}$$

$$g_m^{(iter,AGE)} = g_m^{(iter-1),AGE} \times \omega_g \tag{28}$$

where $\vec{G}_m^{(iter,AGE)}$ is assigned to the identification of the motion parameter of the ith horse, and exemplifies the capability to graze for the appropriate horse.

This parameter decreases linearity with ω_g per iteration of the algorithm. The grazing space is restricted between its upper limit $\tilde{u}$ and the lowest limit $\tilde{l}$. p is a number chosen arbitrarily in the interval [0, 1].

- Hierarchy (H):

The life of horses in groups is often governed by the theory of dominance, formerly referred to as hierarchical order. Under natural conditions, a hierarchy in groups of horses is essential for finding food resources and, above all, avoiding predation. However, the co-ordination of activities, regardless of differences in individual motivations or physiological needs, would be their first priority. The hierarchical order is established and implemented by a series of well-determined behaviors and/or aggressive contact and in relation to several criteria that may govern hierarchical rank, such as age, weight, group size, stability, and duration of group membership of each member. Thus, a group of horses necessarily has a leader who acts as a decision trigger.

Based on collective motions, it has been shown that group members aged between 5 and 15 (i.e., at β and γ ages) are the most motivated and committed to pursuing the individual acting as leader. The tendency of the horse herd members to follow the leadership horse's decisions is represented by the coefficient h_m according to Equations (29) and (30):

$$\vec{H}_m^{(iter,AGE)} = h_m^{(iter,AGE)}[X_*^{(iter-1)} - X_m^{(iter-1)}], \quad AGE = \alpha, \beta and \gamma \tag{29}$$

$$h_m^{(iter,AGE)} = h_m^{(iter-1),AGE} \times \omega_h \tag{30}$$

Herein, $X_*^{(iter-1)}$ illustrates the position of the horse qualified as the best and $H_m^{(iter,AGE)}$ simulates how this parameter (best location of the horse) affects the velocity parameter.

- Sociability (S):

Horse social relationships are well established by setting up social statuses that guarantee herd stability and keep strong, aggressive behavior to a minimum, therefore reducing the risk of injury and loss of energy, as well as facilitating escape from predators and increasing their chances of survival. Although horses live in groups, where those aged 5 to 15 are the most eager to belong to the herd, they are also generally open to other herds, such as cattle and sheep, and willing to live with them. This is clearly shown by Equations (31) and (32).

$$\vec{S}_m^{(iter,AGE)} = S_m^{(iter,AGE)} \left[\left(\frac{1}{N} \sum_{j=1}^{N} X_j^{(iter-1)} \right) - X_m^{(iter-1)} \right], \quad AGE = \beta and \gamma \tag{31}$$

$$s_m^{(iter,AGE)} = s_m^{(iter-1),AGE} \times \omega_s \tag{32}$$

N shows the horse population, and AGE is the age range of each member of the horse herd. $s_m^{(iter,AGE)}$ is related to the orientation of the ith horse toward the direction of the horse group. This variable decreases with the ω_s factor in each execution cycle. Accordingly, $\vec{S}_m^{(iter,AGE)}$ denotes the ith horse social motion vector. At this stage, the determination of the coefficients s for the horses belonging to β and γ categories can be derived.

- Imitation (I):

Imitation behavior is considered one of the most important forms of social learning acquired by horses. It is a behavior that depends on one individual observing another's behavior and repeating it, therefore influencing the observer's motivational state, eliciting and implementing a response, and thus transferring behaviors between the herd members. In most cases, the younger horses in the herd learn from the adult members through good socialization and imitation of their behavior. In the HHO algorithm, this factor, noted i, has been included and mathematically equated as in (33) and (34):

$$\vec{I}_m^{(iter,AGE)} = i_m^{(iter,AGE)} \left[\left(\frac{1}{pN} \sum_{j=1}^{pN} \hat{X}_j^{(iter-1)} \right) - X^{(iter-1)} \right], \quad AGE = \gamma \tag{33}$$

$$I_m^{(iter,AGE)} = i_m^{(iter-1),AGE} \times \omega_i \tag{34}$$

If we consider that 10% (p parameter) of the horses are in the best position and that ith horse is moving towards the best positions $\hat{X}$ of the average horses, then $\vec{I}_m^{(iter,AGE)}$ is the movement vector of the ith horse toward $\hat{X}$ position. ω_i is a per-cycle reducing factor for ith iteration.

- Defense mechanism (D):

Horses are social animals and have a prey status in the wild. For this reason, they prefer to live in large areas with unobstructed visibility so they are always on the lookout for attacks from potential predators and can alert the group. Essentially, the horse's first instinctive defense mechanism is escape, followed by fighting in other circumstances when being hunted.

The defense system is present in the horse, whatever its age, and is manifested on the one hand by instinctive flight from the source of danger when observing unfamiliar behavior on the part of one or more members of the herd and, on the other hand, by the fight against predators. The characterization of such a mechanism is assumed by a negative factor d according to the following Equations (35) and (36):

$$\vec{D}_m^{(iter,AGE)} = -d_m^{(iter,AGE)}\left[\left(\frac{1}{qN}\sum_{j=1}^{qN}\hat{X}_j^{(iter-1)}\right) - X^{(iter-1)}\right], \quad AGE = \alpha, \beta and \gamma \tag{35}$$

$$d_m^{(iter,AGE)} = d_m^{(iter-1),AGE} \times \omega_d \tag{36}$$

Assuming that 20% (q parameter) of the horses are in the worst position and that ith horse is running away from the worst positions $\check{X}$ of the average horses, then $\vec{D}_m^{(iter,AGE)}$ is the escape vector of the ith horse toward $\check{X}$ position. ω_d is a per-cycle reducing factor for dth iteration.

- Roam (R):

When grazing on pastures, horses move extensively, around 16 km per 24 h on pasture. Grass is the preferred feed for horses. The importance of grazing lies in the fact that it brings many benefits: improving the horse's health, as its digestive system is designed to eat continuously, and satisfying its basic need for movement as it moves while eating. In addition, group grazing stimulates competition between herd members to conquer the most fertile grazing areas and compete to discover new zones. In contrast, when the horses are inside the stables, the best design is to allow the horses to see each other. In such circumstances, young horses roam more than mature horses. This behavior has been simulated according to Equations (37) and (38):

$$\vec{R}_m^{(iter,AGE)} = r_m^{(iter,AGE)} p X^{(iter-1)} \quad AGE = \gamma and \delta \tag{37}$$

$$r_m^{(iter,AGE)} = r_m^{(iter-1),AGE} \times \omega_r \tag{38}$$

where $\vec{R}_m^{(iter,AGE)}$ represents the ith horse random velocity vector of the ith horse and ω_r is a per-cycle reducing factor for $r_m^{(iter,AGE)}$.

2.4.2. Proposed Chaotic HHO (CHHO) Algorithm

By analogy with the theory of relativity and quantum mechanics, chaos theory has been one of the great scientific revolutions of the 20th century since it first emerged, leading to a multidisciplinary paradigm shift. Since the 1970s, this theory has made it possible to study nonlinear phenomena governed by simple, deterministic laws whose behavior becomes unpredictable under most conditions.

For nonlinear dynamic systems, chaos can be considered to be a deterministic random process characterized by its significant sensitivity to initial conditions. Indeed, a significant change can occur in the behavior of this type of system, even for a small deviation in the initial values. Thus, the fine internal structure of chaos enables us to attribute important dynamic characteristics to chaotic systems. These characteristics revolve specifically around determinism, randomness, and sensitivity to initial conditions. In relation to optimization algorithms, the aforementioned properties enable population diversity to be maintained, and consequently, the chaotic systems succeed in improving the quality of the global optimum search and escaping falling into a local optimum when dealing with complicated problems.

The consideration of the chaos concept as a discrete-time dynamic system is expressed by:

$$cp_{k+1}^{i} = f(cp_k^i), n = 1, 2, 3, 4, \ldots n \tag{39}$$

where n is the map dimension. $f(cp_k^i)$ is the function described by one of the maps and is used to generate the chaotic model.

In the present work, ten uni-dimensional chaotic maps have been examined to enhance the traditional HHO. For the considered maps, the main parameters and expressions are given in Equations (40)–(50).

Taking into account the parameters $a = 0.5$ and $b = 0.2$, the expression of the Circle map is established by (40) to:

$$x_{n+1} = x_n + b - \left(\frac{a}{2\pi}\right) \sin(2\pi x_n) \bmod (1) \tag{40}$$

The Logistic map is as in Equation (41). $a = 0.4$ is taken.

$$x_{n+1} = a x_n (1 - x_n) \tag{41}$$

The Chebyshev map is expressed as in Equation (42).

$$x_{n+1} = cos(kcos^{-1} x_n) \tag{42}$$

The Gauss/mouse map is expressed by:

$$x_{n+1} = \left\{ \begin{array}{cc} 0, & x_n = 0 \\ \frac{1}{x_n \bmod (1)}, & x_n \in (0,1) \end{array} \right\}, \frac{1}{x_n \bmod (1)} = \frac{1}{x_n} - \left\lfloor \frac{1}{x_n} \right\rfloor \tag{43}$$

The Piecewise map, when adopting $P = 0.4$, is as follows (44).

$$x_{n+1} = \left\{ \begin{array}{c} \frac{x_n}{P}, 0 \le x_n < P \\ \frac{x_n - P}{0.5 - P}, P \le x_n < 0.5 \\ \frac{1 - P - x_n}{0.5 - P}, 0.5 \le x_n < 1 - P \\ \frac{1 - x_n}{P}, 1 - P \le x_n < 1 \end{array} \right\} \tag{44}$$

By fixing the parameter $a = 0.7$, the Iterative map can be defined following to the Equation (45).

$$x_{n+1} = \sin\left(\frac{a\pi}{x_n}\right) \tag{45}$$

The Singer map is expressed by Equation (46) when $\mu = 1.07$.

$$x_{n+1} = \mu\left(7.86x_n - 23.31x_n^2 + 28.75x_n^3 - 13.302875x_n^4\right) \tag{46}$$

The Tent Map is given by Equation (47).

$$x_{n+1} = \left\{ \begin{array}{c} \frac{x_n}{0.7}, x_n < 0.7 \\ \frac{10}{3x_n(1 - x_n)}, \text{ otherwise} \end{array} \right\} \tag{47}$$

The Sine map is represented as in Equation (48), with $a = 4$.

$$x_{n+1} = \frac{a4}{\sin}(\pi x_n), for(0 < a \leq 4) \tag{48}$$

The Sinusoidal map is given by the relation (49).

$$x_{n+1} = a x_n^2 \sin(\pi x_n) \tag{49}$$

When selecting $x_0 = 0.7$ and $a = 2.3$, Equation (49) is rewritten as in (50):

$$x_{n+1} = \sin(\pi x_n) \tag{50}$$

After many tests, only the Tent Map is retained for the investigation of the CHHO performance when utilized for the PVWPS control. A detailed description of the MPPT-based CHHO is shown in the flowchart Figure 5.

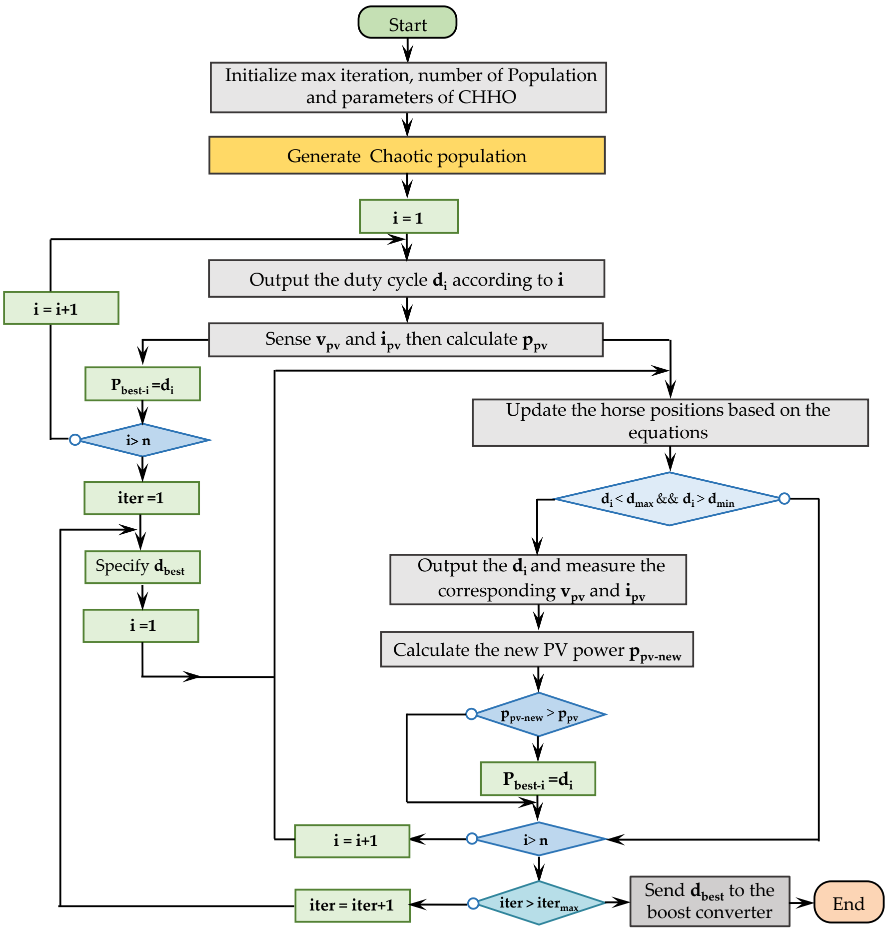

Figure 5. Flowchart of the MPPT-based CHHO.

At this point, the duty cycle of the DC–DC chopper is adjusted by the proposed CHHO algorithm so that the PV generator operates at the point of maximum power, and the maximum available power is therefore transferred to the DC bus before being converted by the VSI to supply the motor and pump.

3. Simulation and Results Analysis

This section is devoted to unveiling the results of the simulations carried out and their associated analyses. To highlight the consistency of the CHHO theory, three precisely specified scenarios have been processed.

3.1. In Absence of Partial Shading

The main objective of the first study is to assess the performance of P&O, PSO, HHO, and CHHO-based MPPT strategies. The evaluations were carried out for the first scenario under standard test conditions (STC) with a solar irradiance of 1000 W/m^2, allowing a maximum power (P_{pv}) of 2000 W generated by the photovoltaic array. Figure 6 shows the results of the generated PV power and the chopper output power (P_{out}) obtained by the MPPT techniques based on the algorithms P&O (Figure 6a), PSO (Figure 6b), HHO (Figure 6c) and CHHO (Figure 6d).

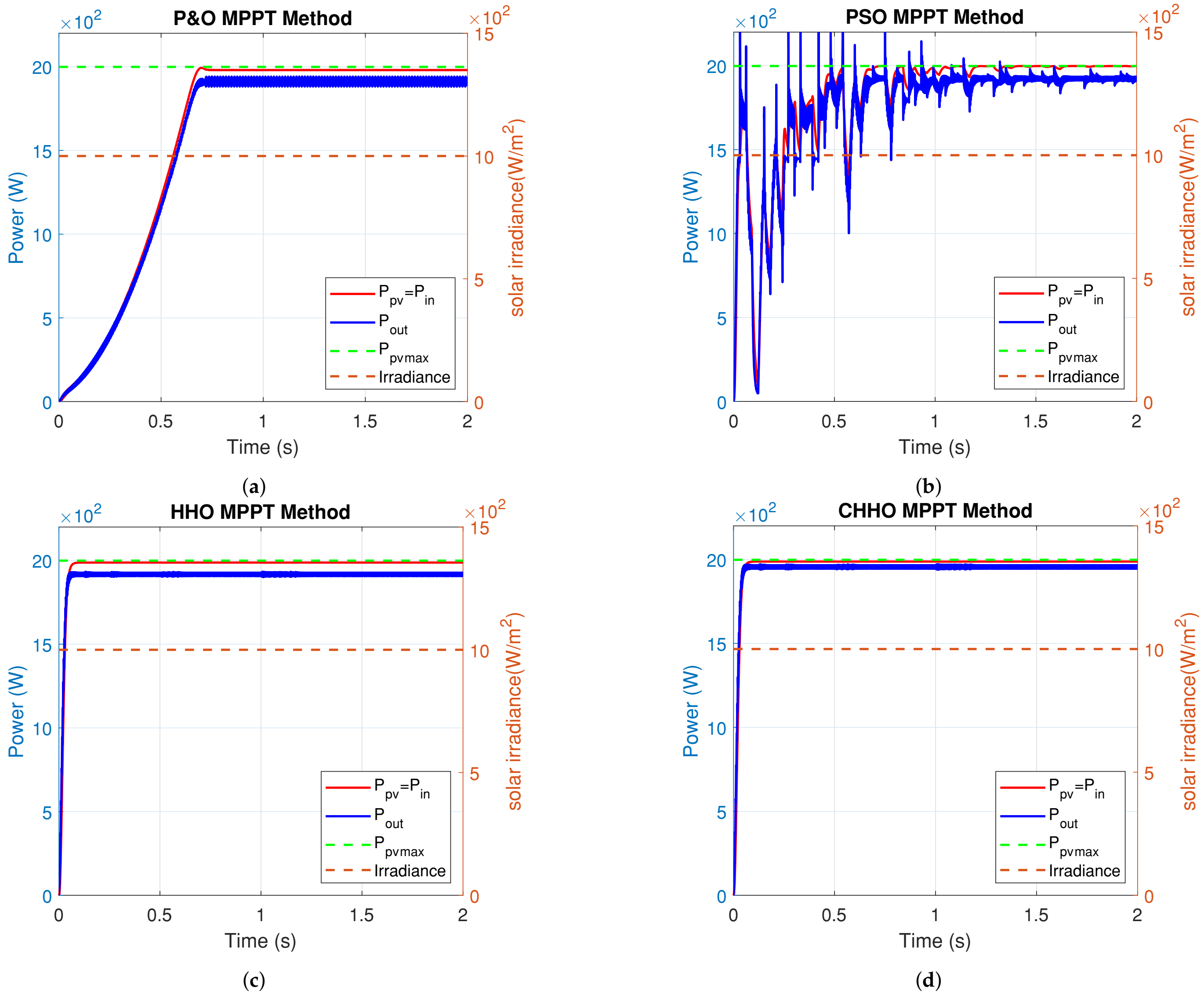

Figure 6. Photovoltaic power and inverter output power for different MPPT strategies at 1000 W/m^2. (**a**) P and O MPPT Method. (**b**) PSO MPPT Method. (**c**) HHO MPPT Method. (**d**) Proposed MPPT Method (CHHO).

At first glance, it can be seen that all MPPT algorithms satisfactorily maintain the voltage close to the Maximum Power Point (MPP). However, by reducing the scale from 1985 to 2050 W (See Figure 7a,b), it becomes clearer to realize that the proposed strategy achieves a remarkable efficiency of 98%. In descending order, it is closely followed by the HHO (96%), PSO (95%), and P&O (94.5%) methods. In terms of processing speed, the proposed MPPT control algorithm (CHHO) is outstanding, as it converges to the MPP in less than 0.08 s, while the PSO and P&O algorithms require 0.7 s and slightly more than

0.08 s, respectively. Compared to the original HHO, the CHHO clearly demonstrates how rapidly convergence has emerged as the superior technology for tracking the MPP.

Another point of interest for benchmarking purposes is that stabilization is directly affected by voltage and current fluctuations at the converter terminals. In addition, MPPT control using the proposed CHHO metaheuristic approach offers higher stability with fewer power oscillations and, therefore, less stress on the switching devices of the DC–DC converter. Furthermore, the proposed CHHO control appears to be more robust under transient conditions than competitive techniques, especially PSO, which exhibits severe power and voltage drops at the start of the MPPT search (Figure 6b).

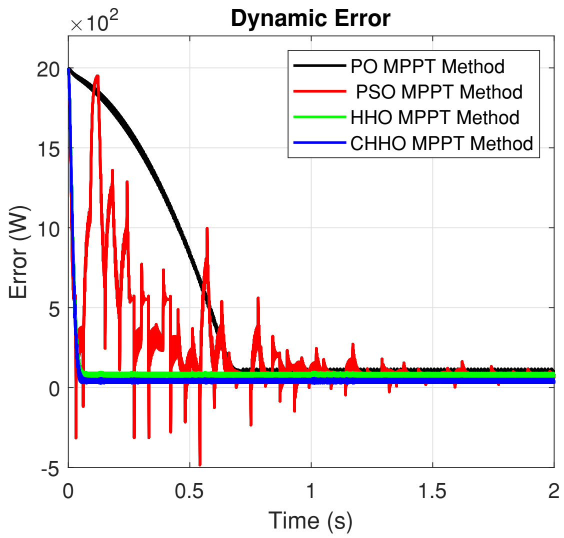

(**a**)

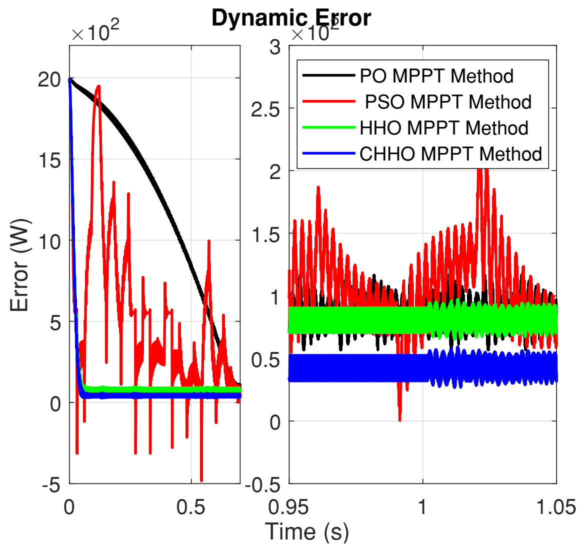

(**b**)

Figure 7. Comparison of results from the proposed MPPT method (CHHO) and the other methods. (**a**) Dynamic error. (**b**) Zoom effect.

3.2. In Case of Partial Shading Conditions

To further confirm the performance and precision of the proposed MPPT algorithm compared to the other three algorithms, P&O, PSO, and HHO, a second benchmarking study was carried out under partial shading condition (PSC). In fact, at a constant temperature of 25 °C, three of the eight photovoltaic modules used were subjected to three irradiance levels distinct from those of the other ones assumed to be subject to the nominal irradiance of 1000 W/m^2. The three levels of shading considered are 400 W/m^2 for PV module 1, 900 W/m^2 for PV module 2 and 300 W/m^2 for PV module 5 (See Figure 8).

Under these conditions, the P-V curve, illustrated in Figure 9, shows that the photovoltaic generator has three local maximum power points (LMPPs) of 1234.8 W, 805.9 W and 684.8 W and a single global MPP (GMPP) corresponding to the power 1422.3 W.

Figure 10 illustrates the dynamic response of the DC–DC converter output power for the different MPPT strategies. Under the partial shading conditions, three algorithms succeeded in finding the GMPP (Figure 10b–d). Referring to the reference GMPP value of 1422.3 W, the CHHO algorithm reached a power level of 1418.8 W, while the HHO and PSO algorithms reached 1403.5 W and 1400.9 W, respectively. Consequently, it is asserted that the CHHO algorithm outperformed the other methods in achieving the GMPP. On the other hand, Figure 10a shows that the P&O algorithm became stuck in an LMPP of 802.1 W, resulting in significant power losses.

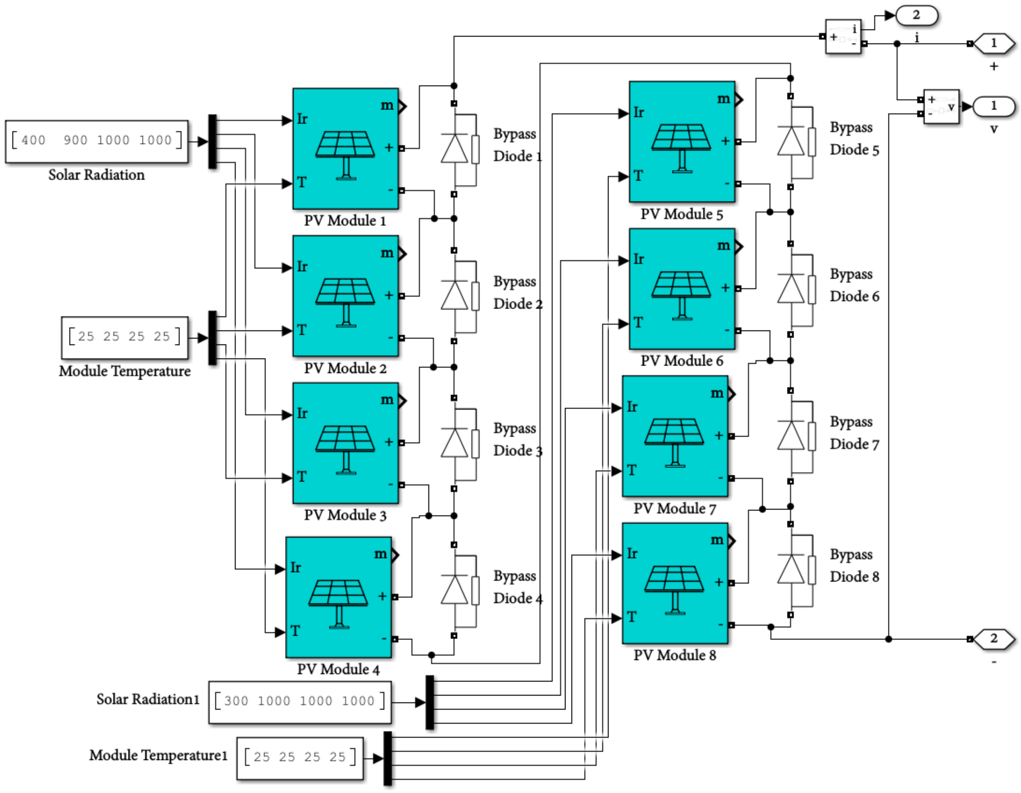

Figure 8. Photovoltaic array configuration under PSC.

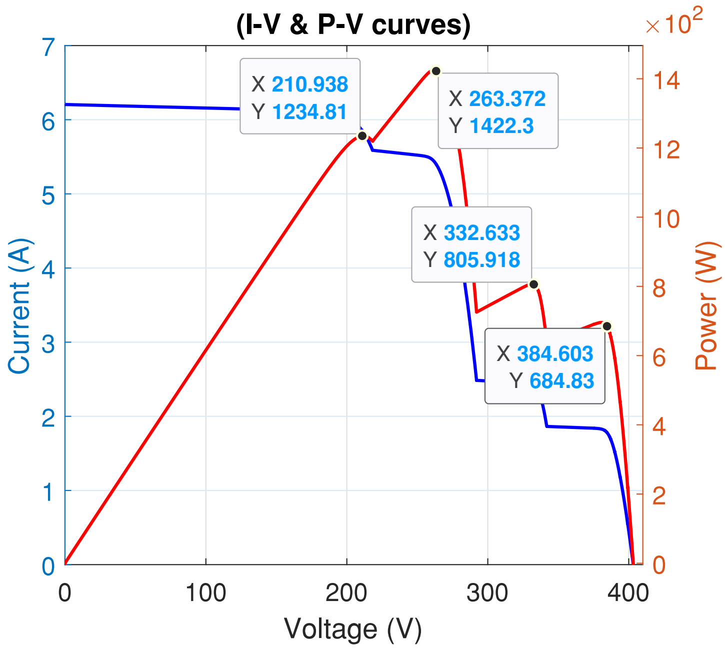

Figure 9. I-V and P-V characteristics of PV array under PSC.

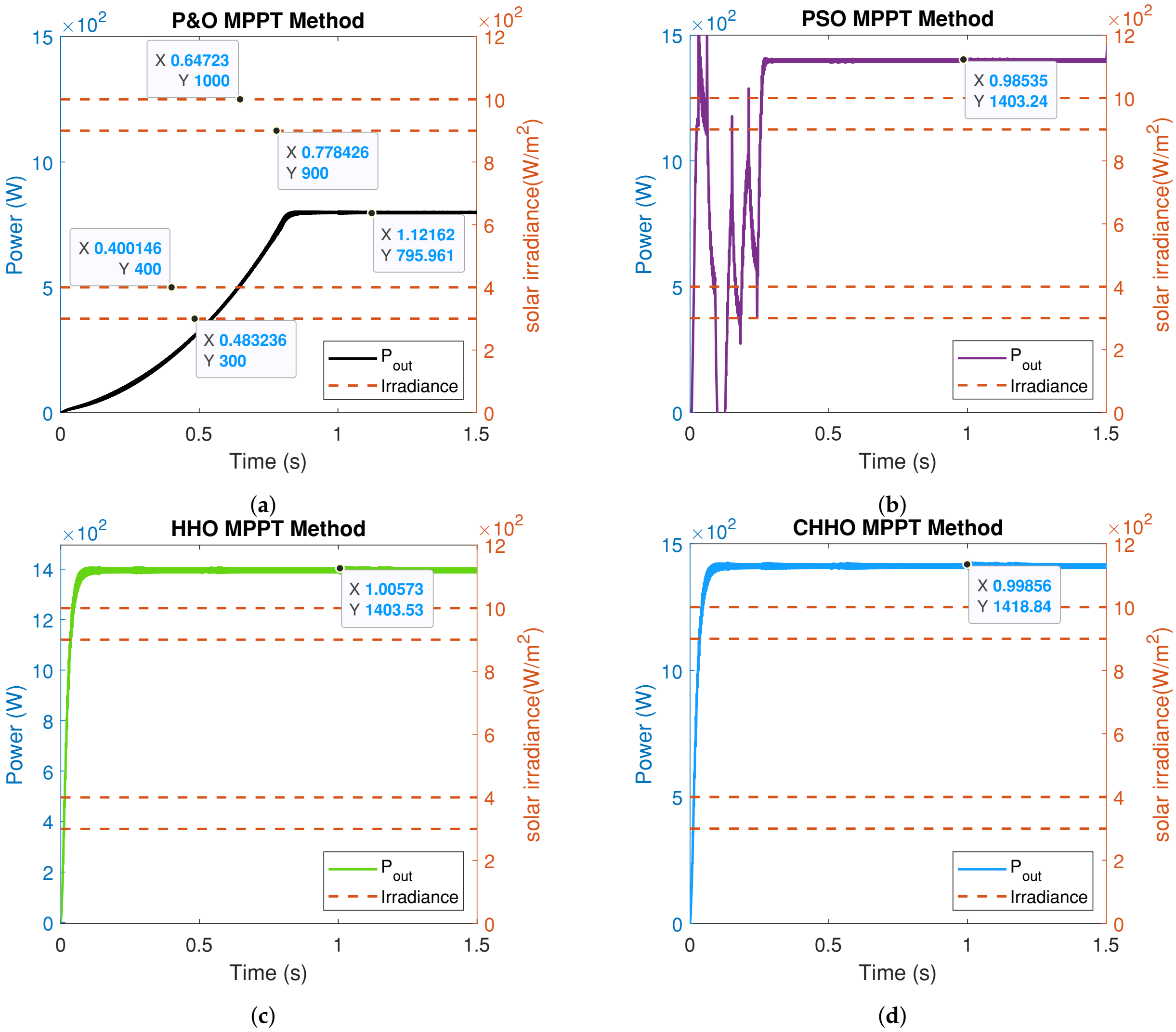

Figure 10. Output power of the boost chopper for different MPPT strategies under PSC. (**a**) P and O MPPT Method. (**b**) PSO MPPT Method. (**c**) HHO MPPT Method. (**d**) Proposed MPPT Method (CHHO).

3.3. Validation of CHHO Dynamic Performance for the SPVWPS

Once the efficiency of the control techniques has been evaluated under standard test conditionsand partial shading conditions, the next objective is to analyze their behavior and performance under transient conditions. Figure 11 shows the results obtained by P&O MPPT (Figure 11a), PSO MPPT (Figure 11b), HHO MPPT (Figure 11c) and the proposed CHHO-MPPT (Figure 11d) methods under sudden irradiation variations: 700, 1000 and 800 W/m^2 at instants of 0, 1.5 and 3 s, respectively. Despite significant variations in solar irradiance, the strategies succeed, with varying degrees of success, in tracking the maximum power point.

After examining the results of simulations of the solar pumping system using the four MPPT techniques under varying irradiation conditions, careful comparisons were made between these methods in terms of response time to reach maximum power and power oscillations around the MPP. The results of the tests corresponding to 700, 1000, 800 W/m^2 are presented in Table 4. Based on the observation of the cases reported there, CHHO-MPPT can provide the least power oscillations and the best response time compared to other MPPT methods, therefore improving system performance.

At this stage, the study was extended to cover the impact of CHHO control performance on the behavior of the whole SPVWPS system. The simulation results shown in

Figure 12 represent the temporal evolutions in a dynamic regime of the power delivered by the PVG, as well as the speed response, the electromagnetic torque of the motor, and the pump flow rate when the proposed CHHO-MPPT is implemented under different irradiation (400, 800, 1000, 800 and 500 W/m^2). The variation period is set at 1*s*.

The temporal evolution of the maximum power extracted from the photovoltaic generator is shown in Figure 12b. It can be seen that a decrease or increase in solar irradiation leads to a decrease or increase, respectively, in the photovoltaic power output. As a result, the maximum power point reached by the control system shifts to match the new maximum power point associated with this new irradiation value. This means that the CHHO algorithm can continuously determine the new optimum voltage for maximum power. As with power, Figure 12d shows that the rotation speed takes on a value of 47.6 rad/s for an irradiance of 400 W/m^2 before, in turn, it undergoes an increase, at time t = 2 s, to reach a value of 156. A total of 434 rad/s, which corresponds to 1000 W/m^2, then reaches a value of 73.43 rad/s at t = 4 s for sunshine of 500 W/m^2.

As for the flow of pumped water, its value reaches 1.6×10^{-4} m^3/s, before increasing to 5.2×10^{-4} m^3/s after 2 s; then 2.4×10^{-4} m^3/s after 4 s. This variation is necessarily imposed by the increase or decrease in the value of the irradiance (see Figure 12f).

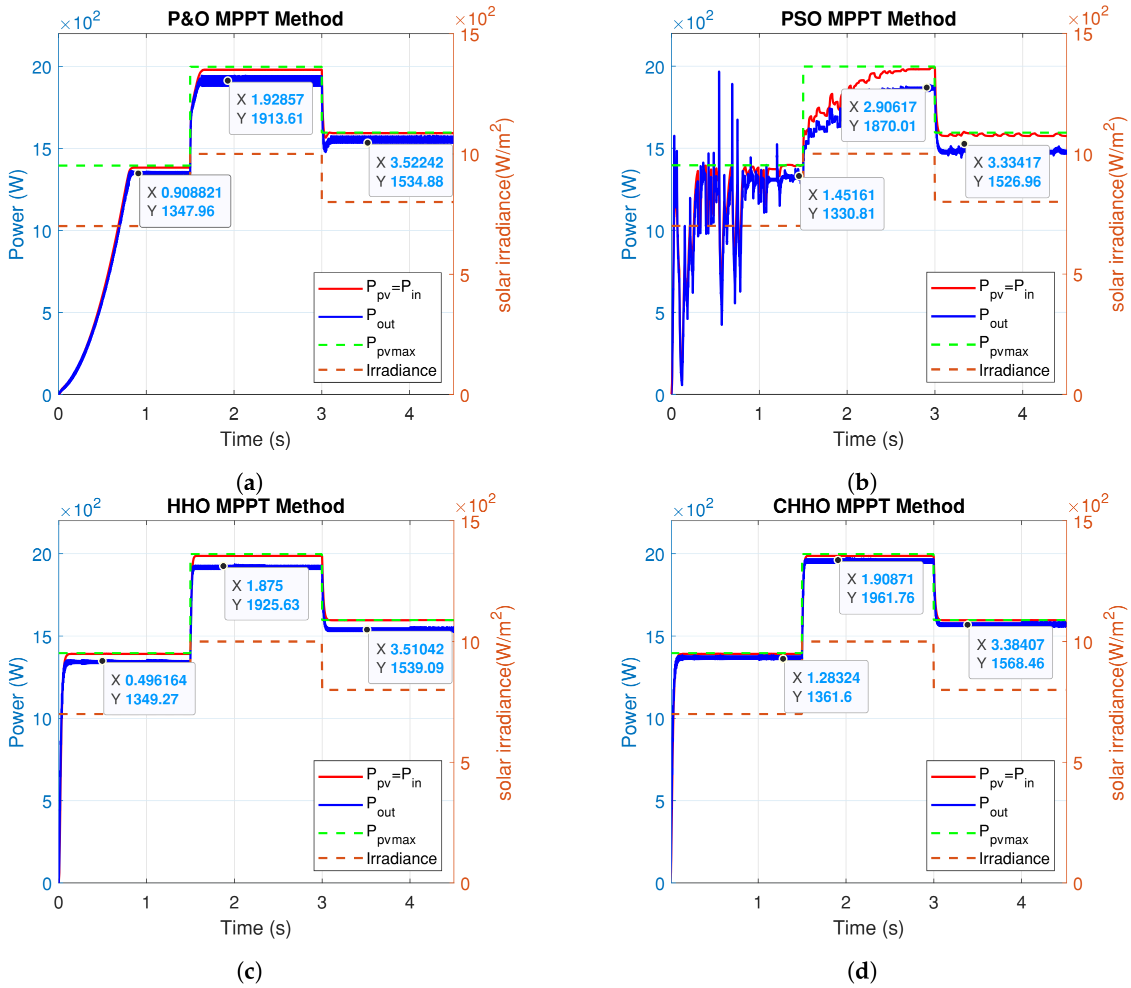

Figure 11. Photovoltaic power and output power of the chopper for different MPPT strategies under variable solar radiation. (**a**) P and O MPPT Method. (**b**) PSO MPPT Method. (**c**) HHO MPPT Method. (**d**) Proposed MPPT Method (CHHO).

Table 4. Comparison results for P&O, PSO, HHO, and CHHO techniques during variable irradiance.

Irradiance (W/m^2)	Features	MPPT Techniques			
		P&O	PSO	HHO	Proposed CHHO
700	Response Time (s) Power oscillations (w)	00.70 16.00	00.35 22.000	00.08 10.00	00.04 07.00
1000	Response Time (s) Oscillations Power (w)	00.10 23.00	00.70 33.00	00.035 18.00	00.02 13.75
8000	Response Time (s) Oscillations Power (w)	00. 16 18.00	00.07 26.00	00.04 14.00	0.025 08.50

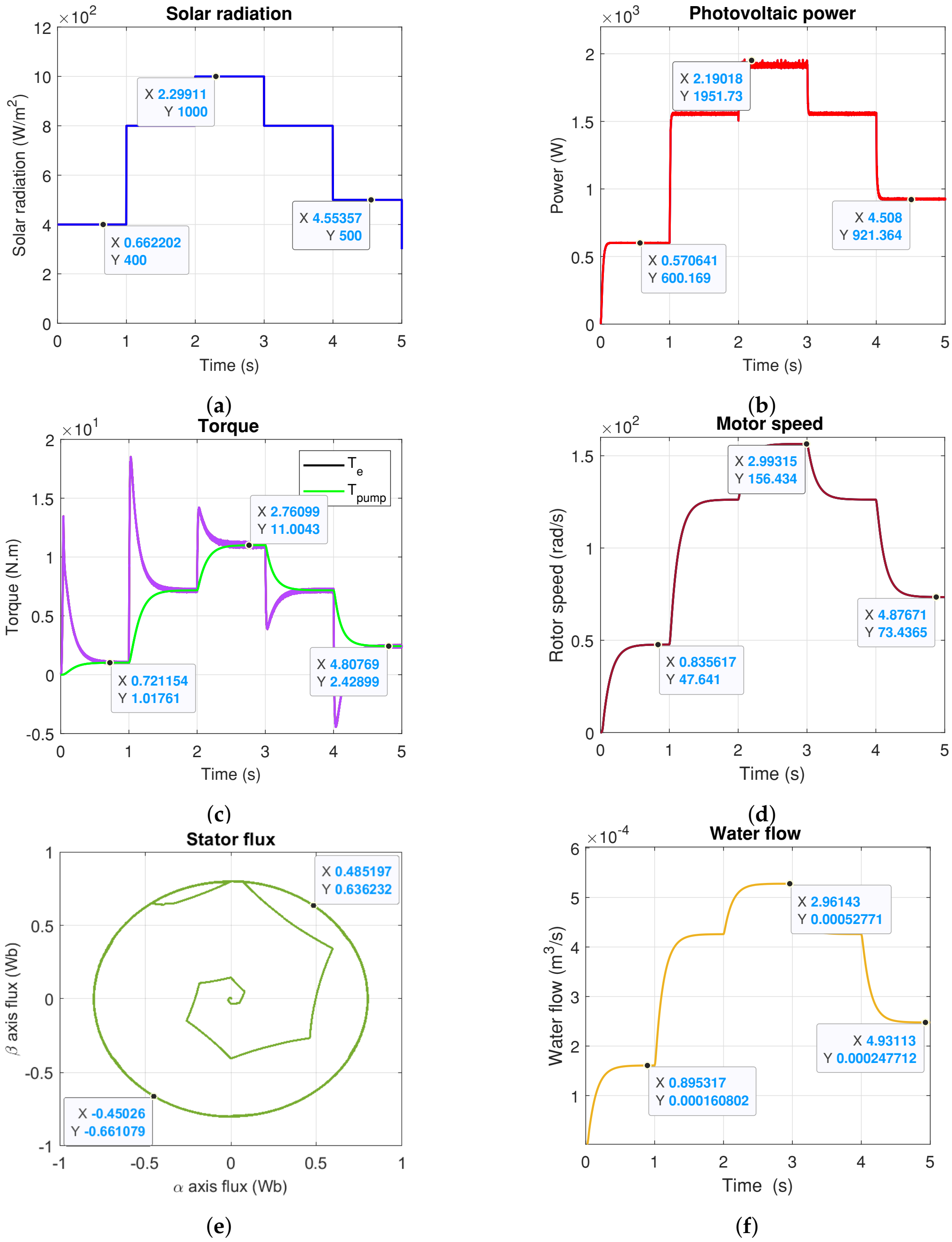

Figure 12. Simulation result of the Photovoltaic Water Pumping System using DTC and the proposed MPPT Method. (**a**) Solar irradiance trajectory. (**b**) PV power trajectory. (**c**) Electromagnetic torque and the pump torque. (**d**) Motor speed trajectory. (**e**) Flux circular Trajectory. (**f**) Water flow.

By examining Figure 12c, it is obvious that the torque T_{pump} reaches a value of 1.01 N·m before rising at t = 2 s (11 N·m), then 4 s (2.42 N·m). The developed electromagnetic torque T_e, in turn, perfectly follows the pump's resistive torque T_{pump} at each change in irradiance.

Otherwise, the stator flux vector follows its reference perfectly and describes a quasi-circular trajectory and only negligible flux fluctuations are registered (see Figure 12e).

4. Conclusions

This paper proposed a new control system for PVWPS. The studied system integrates a PV generator supplying an induction motor and a centrifugal pump via an MPPT-controlled DC–DC chopper and DC-AC voltage source inverter responsible for the DTC control of the IM. In particular, the MPPT process has been ensured by a newly proposed CHHO-based approach under partial shading conditions and fast weather-changing regimes. The MPPT task has been treated as an optimization problem, and the proposed CHHO-based method has been compared with the P&O, PSO, and the original HHO methods. The results of the statistical simulation confirm that the proposed CHHO-based algorithm has excellent advantages compared to other benchmark algorithms in terms of accuracy, reliability, and convergence speed. Especially for PVWPS applications, the whole control system is promising and can be a valuable tool for optimizing the use of AI and metaheuristics to control renewable energy in the promotion of sustainable agriculture, as it achieves better performance in tackling the nonlinear equations of the investigated maximum power point tracking problem. This study can help companies, governments, and nongovernmental organizations better take into account the variability and sustainability of groundwater resources in the optimal sizing and monitoring of PVWPS.

In the continuity of this work, it would be worthwhile to explore and improve the CHHO and other metaheuristic algorithms for further benefits in this sustainable application and other renewable energy and power systems.

Author Contributions: All authors (R.A. and S.S.) contributed equally. All authors have read and agreed to the published version of the manuscript.

Funding: This research was funded by the Scientific Sheikh Ali Mohamed Al-Jumaia Chair on Sustainable Development in Agricultural Societies at the University of Ha'il—Saudi Arabia through Project Number SCR-22 104.

Data Availability Statement: Data are contained within the article.

Acknowledgments: The authors thank the Editors and Reviewers for their valuable and insightful comments that led to improve the sent version.

Conflicts of Interest: The authors declare no conflict of interest.

Abbreviations

The following abbreviations are used in this manuscript:

RERs	Renewable Energy Resources
PV	Photovoltaic
KSA	Kingdom of Saudi Arabia
P&O	Perturb and Observe
PSO	Particle Swarm Optimizer
HHO	Horse Herd Optimization
CHHO	chaotic Horse Herd Optimization
MPPT	Maximum Power Point Tracking
MPP	Maximum Power Point
MFO	Moth Flame Optimization
EGWO	Extended Grey Wolf Optimizer
SMO	Spider Monkey Optimization
HBO	Honey Badger Optimizer
HPO	Hunter Pray Optimizer

AOA	Arithmetic Optimization Algorithm
PVG	PV Generator
IM	Induction Motor
DTC	Direct Torque Control
VSI	Voltage Source Inverter
PWM	Pulse Width Modulation
MPP	Maximum Power Point
SPVWPS	Solar photovoltaic water pumping system
CO_2	Carbon dioxide
VSS-P&O	Variable Step Size Perturb and Observe
VSS-INC	Variable Step Size Incremental conductance
KF	Kalman filter
SPC-FOCV	Semi Pilot Cell-based Fractional Open Circuit Voltage
PMSM	Permanent Magnet Synchronous Motor
SVM	Space Vector Modulation
RBFNN	Radial basis function neural network
SEPIC	Single-ended primary inductor converter
DC	Direct current
BLDC	Brushless DC
VSI	Voltage source inverter
THD	Total harmonic distortion
PWM	Pulse Width Modulation
STC	Standard test conditions

References

1. IEA: More Than a Third of the World's Electricity Will Come from Renewables in 2025. Available online: https://www.weforum.org/agenda/2023/03/electricity-generation-renewables-power-iea/ (accessed on 15 January 2024).
2. Hoeck, I.; Steurer, E.; Dolunay, Ö.; Helvi, I. Challenges for off-grid electrification in rural areas. Assessment of the situation in Namibia using the examples of Gam and Tsumkwe. *Energy Ecol. Environ.* **2021**, *7*, 508–522. [CrossRef]
3. Arash, F.S.; Saeed, D.M.; Araceli, S. Farm electrification: A road-map to decarbonize the agriculture sector. *Electr. J.* **2022**, *35*, 107076.
4. Ahssein, Y.H.; Mugahed, Y.H.; Rayed, A.; Hisham, A. Renewable and sustainable energy production in Saudi Arabia according to Saudi Vision 2030; Current status and future prospects. *J. Clean. Prod.* **2020**, *247*, 119602.
5. Abdulrahman, M.A.; Ahmed, I.H.; Faleh, A.A. Assessment of farmers practices to date palm soil fertilization and its impact on productivity at Al-Hassa oasis of KSA. *Saudi J. Biol. Sci.* **2021**, *28*, 1451–1458.
6. Abdullahi, A.M. Comparison of three machine learning models for the prediction of hourly PV output power in Saudi Arabia. *Ain Shams Eng. J.* **2022**, *13*, 101648.
7. Houda, B.; Latifa, D.; Riheb, H.; Younes, H.; Hatem, J. Ecologic and economic perspectives for sustainable irrigated agriculture under arid climate conditions: An analysis based on environmental indicators for southern Tunisia. *J. Afr. Earth Sci.* **2021**, *177*, 104134.
8. Upeksha, C.; Ayesha, S.; Ashish, G.; Christian, B. Irrigation efficiency and renewable energy powered desalination as key components of Pakistan's water management strategy. *Smart Energy* **2021**, *4*, 100052.
9. Luis, V.; Maichel, M.A.; Luis, M.; Carlos, O. A MILP-based operational decision-making methodology for demand-side management applied to desalinated water supply systems supported by a solar photovoltaic plant: A case study in agricultural industry. *J. Clean Prod.* **2022**, *334*, 130123.
10. Everest, B. Willingness of farmers to establish a renewable energy (solar and wind) cooperative in NW Turkey. *Arab. J. Geosci.* **2021**, *14*, 157. [CrossRef]
11. Mahto, R.; Sharma, D.; John, R.; Putcha, C. Agrivoltaics: A Climate-Smart Agriculture Approach for Indian Farmers. *Land* **2021**, *10*, 1277. [CrossRef]
12. Ravichandran, N.; Ravichandran, N.; Panneerselvam, B. Floating photovoltaic system for Indian artificial reservoirs—An effective approach to reduce evaporation and carbon emission. *Int. J. Environ. Sci. Technol.* **2022**, *19*, 7951–7968. [CrossRef]
13. Mazhar, A.; Rashid, W.; Kashif, I.; Kafait, U.; Abdul Kashif, J.; Abasin, U.; Abraiz, K.; Joseph, M.G. Techno-economic assessment and sustainability impact of hybrid energy systems in Gilgit-Baltistan, Pakistan. *Energy Rep.* **2021**, *7*, 2546–2562.
14. Irfan, M.; Zhao, Z.; Ahmad, M.; Rehman, A. A Techno-Economic Analysis of Off-Grid Solar PV System: A Case Study for Punjab Province in Pakistan. *Processes* **2019**, *7*, 708. [CrossRef]
15. Rahmani, A.; Naeini, A.B. predicting intention in applying solar energy technologies in agriculture industry: A moderated and mediated model. *Clean. Responsible Consum.* **2023**, 8, 100102. [CrossRef]
16. Abbassi, R.; Marrouchi, S.; Saidi, S.; Abbassi, A.; Chebbi, S. Optimal Energy Management Strategy and Novel Control Approach for DPGSs Under Unbalanced Grid Faults. *J. Circuits Syst. Comput.* **2019**, *28*, 1950057. [CrossRef]

17. Farooq, A.; Wu, X. Review of edutainment immersive visualization (IV) development tools for simulating renewable energy systems (RESs). *Energy Strategy Rev.* **2022**, *44*, 101000. [CrossRef]
18. Pereira, F.; Caetano, N.S.; Felgueiras, C. Increasing energy efficiency with a smart farm—An economic evaluation. *Energy Rep.* **2022**, *8*, 454–461. [CrossRef]
19. Sangeetha, B.P.; Kumar, N.; Ambalgi, A.P.; Abdul Haleem, S.L.; Thilagam, K.; Vijayakumar, P. IOT based smart irrigation management system for environmental sustainability in India. *Sustain. Energy Technol. Assess.* **2022**, *52*, 101973.
20. Naval, N.; Yusta, J.M. Optimal short-term water-energy dispatch for pumping stations with grid-connected photovoltaic self-generation. *J. Clean Prod.* **2021**, *316*, 128386. [CrossRef]
21. Mohammadinodoushan, M.; Rabeh, A.; Jerbi, H.; Ahmed, F.W.; Ahmed, H.A.; Alireza, R. A new MPPT design using variable step size perturb and observe method for PV system under partially shaded conditions by modified shuffled frog leaping algorithm-SMC controller. *Sustain. Energy Technol. Assess.* **2021**, *45*, 101056. [CrossRef]
22. Guo, S.; Abbassi, R.; Jerbi, H.; Rezvani, A.; Suzuki, K. Efficient maximum power point tracking for a photovoltaic using hybrid shuffled frog-leaping and pattern search algorithm under changing environmental conditions. *J. Clean Prod.* **2021**, *297*, 126573. [CrossRef]
23. Ngo, V.D.B.; Latifi, M.; Rabeh, A.; Houssem, J.; Ohshima, K.; Khaksar, M. Improved krill herd algorithm based sliding mode MPPT controller for variable step size P&O method in PV system under simultaneous change of irradiance and temperature. *J. Frankl. Inst.* **2021**, *358*, 3491–3511.
24. Hassan, T.-U.; Abbassi, R.; Jerbi, H.; Mehmood, K.; Tahir, M.F.; Cheema, K.M.; Elavarasan, R.M.; Ali, F.; Khan, I.A. A Novel Algorithm for MPPT of an Isolated PV System Using Push Pull Converter with Fuzzy Logic Controller. *Energies* **2020**, *13*, 4007. [CrossRef]
25. del Rio, A.; Barambones, O.; Uralde, J.; Artetxe, E.; Calvo, I. Particle Swarm Optimization-Based Control for Maximum Power Point Tracking Implemented in a Real Time Photovoltaic System. *Information* **2023**, *14*, 556. [CrossRef]
26. Silaa, M.Y.; Barambones, O.; Bencherif, A.; Rahmani, A. A New MPPT-Based Extended Grey Wolf Optimizer for Stand-Alone PV System: A Performance Evaluation versus Four Smart MPPT Techniques in Diverse Scenarios. *Inventions* **2023**, *8*, 142. [CrossRef]
27. Chang, C.C.W.; Ding, T.J.; Han, W.; Chai, C.C.; Yam, C.M.; Yian, H.C.; Xin, L.H. Moth flame optimization for the maximum power point tracking scheme of photovoltaic system under partial shading conditions. *Energy Rep.* **2023**, 9, 374-379. [CrossRef]
28. Husain, M.A.; Pingale, S.B.; Khan, A.B.; Minai, A.F.; Pandey, Y.; Dwivedi, R.S. Performance analysis of the global maximum power point tracking based on spider monkey optimization for PV system. *Renew. Energy Focus* **2023**, *7147*, 100503. [CrossRef]
29. Chandrasekharan, S.; Subramaniam, S.; Veerakgoundar, V. Honey badger optimization algorithm based maximum power point tracking for solar photovoltaic systems. *Electr. Power Syst. Res.* **2023**, *221*, 109393. [CrossRef]
30. Korany, E.; Yousri, D.; Attia, H. A.; Zobaa, A.F.; Allam, D. A novel optimized dynamic fractional-order MPPT controller using hunter pray optimizer for alleviating the tracking oscillation with changing environmental conditions. *Energy Rep.* **2023**, *10*, 1819–1832. [CrossRef]
31. Chtita, S.; Derouich, A.; Motahhir, S.; EL Ghzizal, A. A new MPPT design using arithmetic optimization algorithm for PV energy storage systems operating under partial shading conditions. *Energy Convers. Manag.* **2023**, *289*, 117197. [CrossRef]
32. Le, X.C.; Duong, M.Q.; Le, K.H. Review of the Modern Maximum Power Tracking Algorithms for Permanent Magnet Synchronous Generator of Wind Power Conversion Systems. *Energies* **2023**, *16*, 402. [CrossRef]
33. Saady, I.; Karim, M.; Bossoufi, B.; El Ouanjli, N.; Motahhir, S.; Majout, B. Optimization and control of photovoltaic water pumping system using kalman filter based MPPT and multilevel inverter fed DTC-IM. *Results Eng.* **2023**, *17*, 100829. [CrossRef]
34. Hilali, A.; Mardoude, Y.; Essahlaoui, A.; Rahali, A.; El Ouanjli, N. Migration to solar water pump system: Environmental and economic benefits and their optimization using genetic algorithm Based MPPT. *Energy Rep.* **2022**, *8*, 10144–10153. [CrossRef]
35. Ahmed, M.M.; Hassanien, W.S.; Enany, M.A. Modeling and evaluation of SC MPPT controllers for PVWPS based on DC motor. *Energy Rep.* **2021**, *7*, 6044–6053. [CrossRef]
36. Ganapathee, M.; Alavandar, S.; Sowmmiya, U.; Kasinathan, P. Semi-pilot cell based maximum power point tracking and coordinated current control based PMSM drive for standalone solar water pumping system. *J. Process Control* **2022**, *112*, 57–68. [CrossRef]
37. Saidi, S.; Abbassi, R.; Chebbi, S. Power quality improvement using VF-DPC-SVM controlled three-phase shunt active filter. In Proceedings of the IEEE 12th International Multi-Conference on Systems, Signals & Devices (SSD15), Mahdia, Tunisia, 16–19 March 2015; pp. 1–5.
38. Gundogdu, A.; Kizmaz, H.; Celikel, R.; Yilmaz, M. Speed sensorless Adaptive Power Control for photovoltaic-fed water pump using Extended Kalman–Bucy filter. *Energy Rep.* **2023**, *10*, 1785–1795. [CrossRef]
39. Chandra, S.; Gaur, P.; Pathak, D. Radial basis function neural network based maximum power point tracking for photovoltaic brushless DC motor connected water pumping system. *Comput. Electr. Eng.* **2020**, *86*, 106730. [CrossRef]
40. Altimania, M.R.; Elsonbaty, N.A.; Enany, M.A.; Gamil, M.M.; Alzahrani, S.; Alraddadi, M.H.; Alsulami, R.; Alhartomi, M.; Alghuson, M.; Alatawi, F.; et al. Optimal Performance of Photovoltaic-Powered Water Pumping System. *Mathematics* **2023**, *11*, 731. [CrossRef]
41. MiarNaeimi, F.; Azizyan, G.; Rashki, M. Horse herd optimization algorithm: A nature-inspired algorithm for high-dimensional optimization problems. *Knowl.-Based Syst.* **2021**, *213*, 106711. [CrossRef]

42. Refaat, A.; Adnan, Q.A.; Elsakka, M.M.; Elhenawy, Y.; Majozi, T.; Korovkin, N.V.; Elfar, M.H. Extraction of maximum power from PV system based on horse herd optimization MPPT technique under various weather conditions. *Renew. Energy* **2024**, *220*, 119718. [CrossRef]
43. Saidi, S.; Abbassi, R.; Chebbi, S. Quality improvement of shunt active power filter with direct instantaneous power estimator based on Virtual Flux. *Int. J. Control Autom. Syst.* **2016**, *14*, 1309–1321. [CrossRef]
44. Saidi, S.; Abbassi, R.; Amor, N.; Chebbi, S. Passivity-based direct power control of shunt active filter under distorted grid voltage conditions. *Automatika* **2016**, 57, 361–371. [CrossRef]
45. Abbassi, R.; Marrouchi, S.; Ben Hessine, M.; Chebbi, S.; Jouini, H. Voltage control strategy of an electrical network by the integration of the UPFC compensator. *Int. Rev. Model. Simul.* **2012**, *5*, 380–384.
46. Elkholy, M.M.; Fathy, A. Optimization of a PV fed water pumping system without storage based on teaching-learning-based optimization algorithm and artificial neural network. *Sol. Energy* **2016**, *139*, 199–212. [CrossRef]